Article

Use of Eggshell-Catalyzed Biochar Adsorbents for Pb Removal from Aqueous Solution

Dongdong Liu, Zhengkai Hao, Dengqian Chen, Lipeng Jiang, Tianqi Li, Bing Tian, Cuiping Yan, Yuan Luo, Guang Chen, and Hongfu Ai*

Read Online

ACCESS | Metrics & More | Article Recommendations | SI Supporting Information

ABSTRACT: Eggshell is a cheap and environmentally friendly calcium source. In this study, Ca-modified biochar adsorbents (CEA) were prepared by 1:10, 1:2, and 1:1 mass ratio of the eggshell and Eupatorium adenophorum. The CEA-2 sample prepared with a 1:2 mass ratio showed a maximum Pb adsorption capacity (97.74 mg·g^{-1}) at the conditions of an initial pH of 7.0, an adsorbent dosage of 0.5 g·L^{-1}, and a contact time of 8.0 h. The kinetic and isotherm studies indicated that the adsorption process of the CEA-2 sample had monolayer adsorption characteristics, which was controlled together by intraparticle and interface diffusion. Thermodynamic studies indicated that the adsorption process of CEA-2 was spontaneous ($\Delta G^0 < 0$) and endothermic ($\Delta H^0 > 0$). X-ray diffraction and scanning electron microscopy analyses showed a uniform distribution of Ca−Pb precipitation on the CEA-2 surface, which proved that chemical precipitation was the main adsorption mechanism. Fourier transform infrared spectra found that CEA-2 had abundant active groups, especially nitrogen-containing functional groups, which could adsorb Pb through a surface complexation reaction. The Brunauer−Emmett−Teller surface area of CEA-2 was found to be 621 m^2·g^{-1}, and such developed pores could ensure the smooth diffusion of Pb. Finally, the effect of coexisting cation and anion experiment and the cyclic regeneration experiment indicated that CEA-2 had prominent stability and reusability for Pb adsorption.
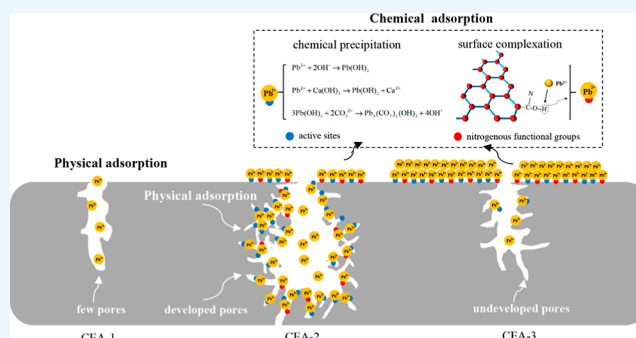
1. INTRODUCTION

Lead (Pb), one of the main pollutants in industrial wastewater, has high toxicity, accumulates easily, and has difficult degradation.[1] The adsorption method has many advantages of simple processing, broad applicability, green environmental protection, and can get rid of heavy metals from wastewater.[2] In previous studies, many researchers have paid more attention to the preparation of traditional adsorbents (such as zeolite, chitosan, pumice, etc.).[3−8] Biochar, as a kind of adsorbent, has the obvious advantages of wide raw material sources, low cost, and a stable physicochemical structure compared to the traditional adsorbents.[9,10] Usually, the biomass feedstock is converted to biochar via a high-temperature treatment (600−800 °C) under an inert atmosphere.[11] However, the biochar prepared from different raw materials (such as switchgrass,[1] woody biomass,[1,12] crofton weed,[13] straw,[14] etc.) has relatively low adsorption capacities of heavy metals. Usually, the biochar has only some undeveloped pores and almost no functional groups after high-temperature treatment. It is difficult for such a physicochemical structure to exhibit excellent adsorption capacity. At present, the metal modification method using potassium (K), iron (Fe), copper (Cu), and magnesium (Mg) is used to improve the physicochemical structure of biochar. Our previous studies explored the effects of Fe-based

compounds on the physicochemical structure of biochar and further confirmed the high adsorption capacity of Fe-modified biochar.[11] Mahdavi et al.[15] prepared a functional biochar using CuO. They found that the addition of a Cu source promoted the affinity of Cu-modified biochar for heavy metals. Li et al.[16] found that the Mg-modified biochar from straw had high adsorption capacities of dyes and heavy metal ions. However, these metal compounds may be released from the adsorbent surface into an aqueous solution during the adsorption process, inevitably causing the secondary pollution and toxic effects.

Calcium (Ca) is an environmentally friendly modifier with non-toxic properties with abundant resources in nature.[17−19] Some studies have found that many materials (such as clinoptilolite, sludge, and biochar) modified by a Ca source have high adsorption capacities for the pollutants from water. Mitrogiannis et al.[20] successfully prepared a zeolite-based adsorbent modified by Ca(OH)$_2$. They found that the
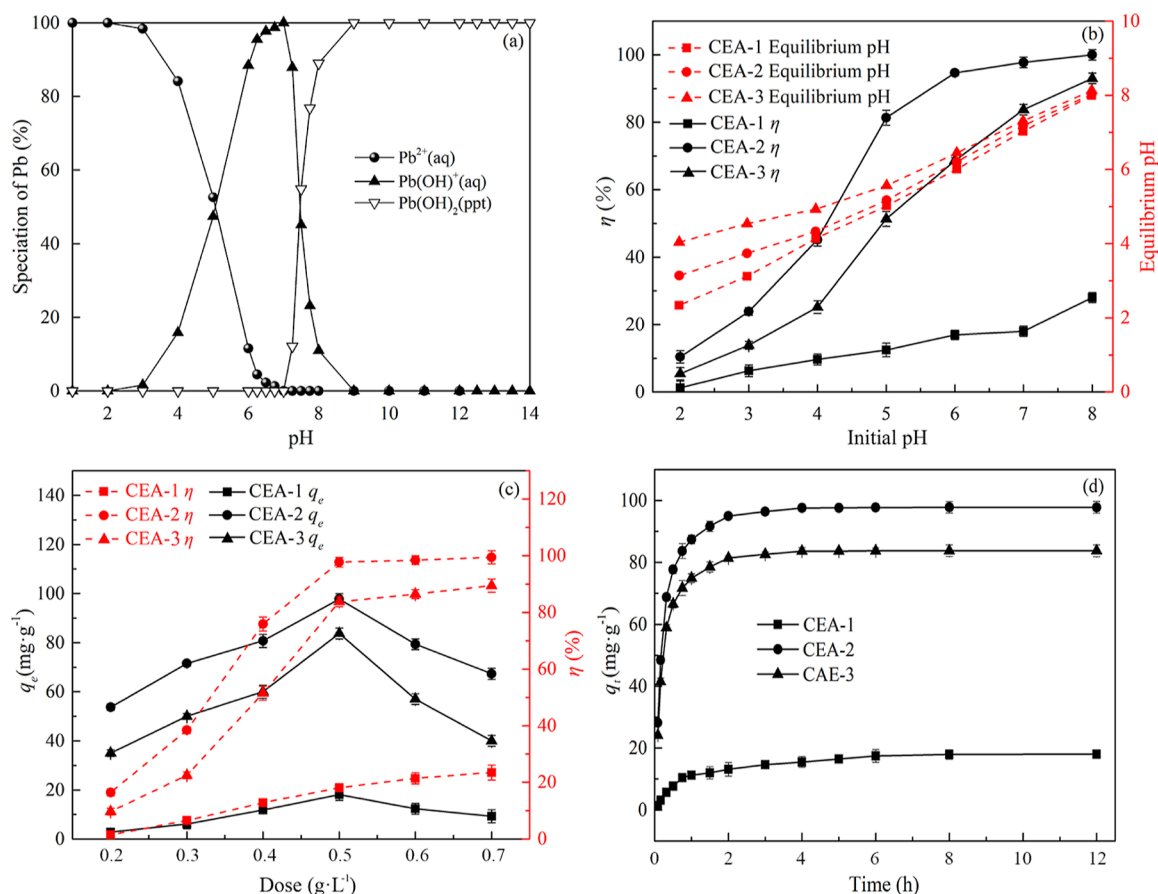
Figure 1. Speciation of Pb species versus pH predicted by the visual MINTEQ 3.1 software (a); effect of initial pH (b), adsorbent dosage (c), and contact time (d) on Pb adsorption onto Ca-modified biochar.

Ca(OH)$_2$-modified adsorbent had high adsorption capacity for phosphate (167.7 mg·g^{-1}). Wang et al.[21] found that CaCl$_2$-modified biochar from the flour showed a maximum adsorption capacity for phosphorus (134.5 mg·g^{-1}). However, the price of a calcium source may limit the actual application of the Ca-modified adsorbent. It is therefore meaningful to study effective alternatives with low cost using biomass waste. Eggshells contain a lot of calcium carbonate (∼94%) and a small part of organic matter (∼6%) and are therefore expected to be an ideal calcium source instead of traditional calcium sources [such as Ca(OH)$_2$, CaCl$_2$, CaCO$_3$, etc.] for the preparation of Ca-modified biochar.[22] To the best of our knowledge, few studies have explored the effect of eggshell modification on the physicochemical structure, Pb adsorption properties, and the mechanism of biochar adsorbent.

Eupatorium adenophorum, a worldwide malignant weed, is a perennial herb with developed roots and ovate or rhombic leaves, and it was introduced into southwest China in 1940s.[23] In addition, it also has the characteristics of high carbon content, strong renewability, and abundant resources. In this study, Eupatorium adenophorum and eggshells were used as the raw material and calcium source, respectively. Three kinds of Ca-modified biochar adsorbents were prepared with different ratios of raw materials and calcium sources. First, suitable conditions including the pH value, dosage, and contact time of three kinds of biochar for Pb adsorption were confirmed, and the corresponding adsorption kinetics, isotherms, and thermodynamic were investigated. Next, the changes in the physicochemical structure of three kinds of

biochar before and after Pb adsorption were systematically evaluated by scanning electron microscopy (SEM), X-ray diffraction (XRD), Fourier transform infrared (FTIR) spectroscopy, and Brunauer–Emmett–Teller (BET) analyses, which clarified the adsorption properties and mechanism of Ca-modified biochar. To explore the potential and extensive applications of Ca-modified biochar adsorbents, the effect of coexisting cation and anion experiment, the mass loss, the adsorption capacity, and the Ca^{2+} release of adsorbents during the desorption regeneration experiment were studied.

2. RESULTS AND DISCUSSION

2.1. Effect of Initial pH, Adsorbent Dosage, and Contact Time. Figure 1a shows the speciation of Pb species at different pH values predicted by visual MINTEQ 3.1 software. The speciation of Pb species was Pb^{2+} under strong acidic conditions (Pb ≤ 2.0), and the Pb species of the solution were the mixture of Pb^{2+} and Pb(OH)$^+$ with the increase of pH value from 2.0 to 7.0. When the pH value was greater than 7.0, Pb precipitates [Pb(OH)$_2$] could be formed in the solution. The effect of initial pH on Pb adsorption of Ca-modified biochar is shown in Figure 1b. The Pb adsorption rate (η) of all three kinds of Ca-modified biochar increased gradually with the increase of initial pH (2.0−8.0), and the η value of CEA-2 was the highest among all samples. The η values of CEA-1, CEA-2, and CEA-3 were 1.27, 10.44, and 5.44% under strong acidic conditions (Pb = 2.0), which might be caused by the competitive adsorption of Pb^{2+} and H$^+$.[24] However, the competitive adsorption of H$^+$ was weakened with the decrease
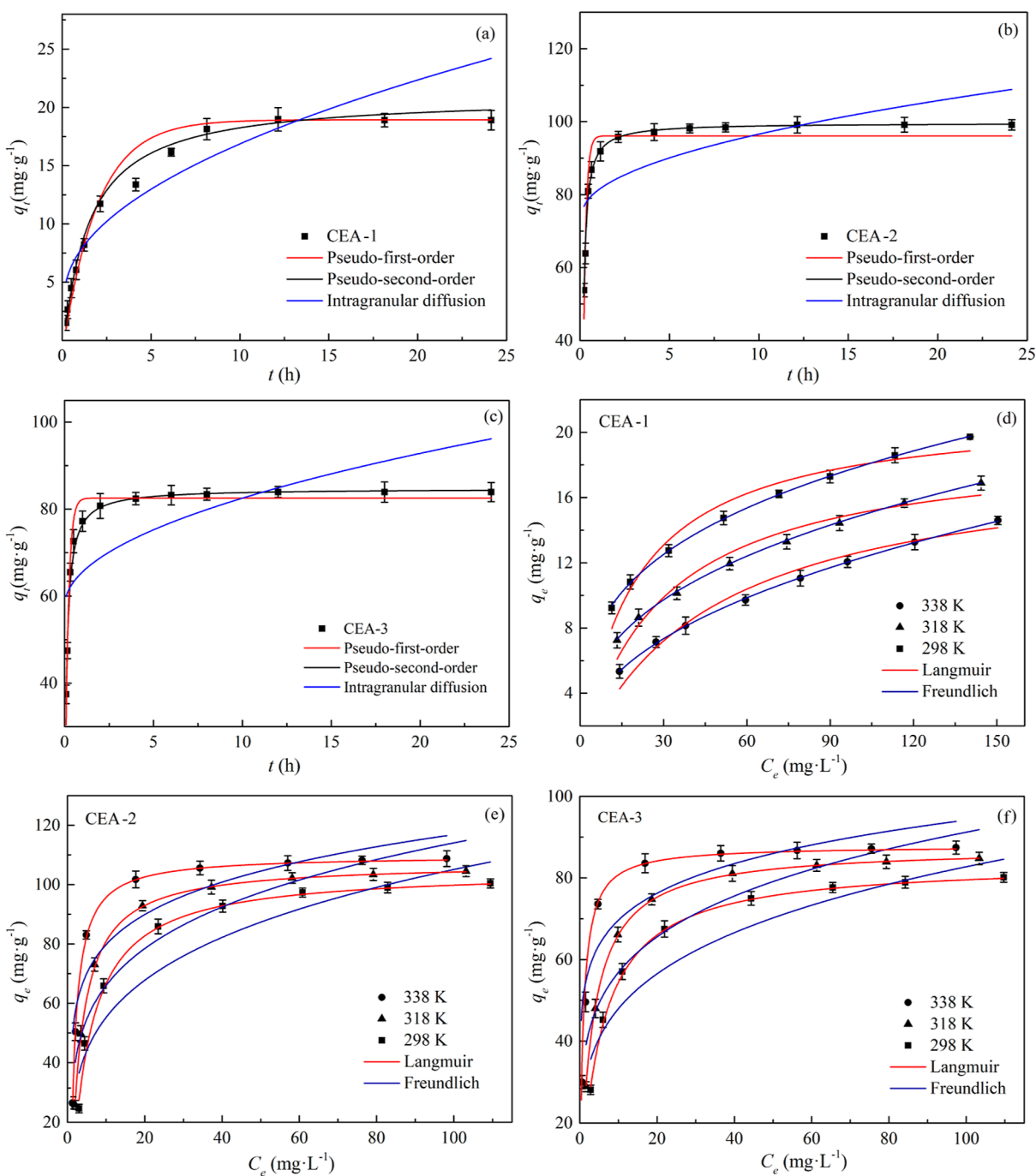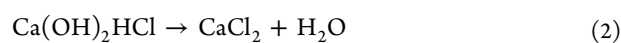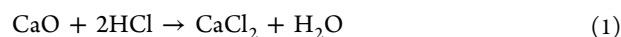
Figure 2. Fitting results of adsorption kinetics (a−c) and isotherms (d−f).

of acidity of the reaction system (pH = 2.0∼7.0), which was conducive to the Pb adsorption of Ca-modified biochar. In addition, the pH_{PZC} values of CEA-1, CEA-2, and CEA-3 were 5.83, 3.63, and 4.01, respectively (Figure S1). When the pH value of the solution was higher than the pH_{pzc} of Ca-modified biochar, the adsorbent surface could become negatively charged through the deprotonation reaction of functional groups, which helped to adsorb the cations [$Pb(OH)^+$ and Pb^{2+}] in the reaction system.[25] Therefore, the η value of CEA-1, CEA-2, and CEA-3 rapidly increased to 18.02, 83.74, and 97.74% at pH = 7.0. However, the continuous increase of η value was mainly related to the formation of Pb precipitates under alkaline conditions (pH = 7.0−8.0). Significantly, the equilibrium pH value of the solution was higher than its initial

pH value, and this difference was more obvious in the ranges of 2.0 and 5.0. In this process, the rise of pH value came from the dissolution of CaO or $Ca(OH)_2$ by H^+ (eqs 1 and 2). As the acidity of the initial solution decreased, the resultant high pH value could be explained by the dissolution of CaO by H_2O (eq 3).

$$CaO + 2HCl \rightarrow CaCl_2 + H_2O \tag{1}$$

$$Ca(OH)_2 HCl \rightarrow CaCl_2 + H_2O \tag{2}$$

$$CaO + H_2O \rightarrow Ca^{2+} + 2OH^- \tag{3}$$

The effect of dosage on Pb adsorption of Ca-modified biochar is given in Figure 1c. Ca-modified biochar had the low

Table 1. Kinetic Parameter of Ca-Modified Biochar for Pb Adsorption

kinetic models	parameters	CEA-1	CEA-2	CEA-3
pseudo-first-order	q_e,exp $(mg \cdot g^{-1})$	18.023 ± 0.42	97.742 ± 1.41	83.731 ± 2.21
	q_e $(mg \cdot g^{-1})$	19.531	96.641	81.758
	k_1 (h^{-1})	0.510	6.660	5.531
	R^2	0.976	0.967	0.904
pseudo-second-order	q_e $(mg \cdot g^{-1})$	21.926	98.960	85.087
	k_2 $(g \cdot mg^{-1} \cdot h^{-1})$	0.074	0.122	0.109
	R^2	0.881	0.993	0.987
intragranular diffusion	C_i $(mg \cdot g^{-1})$	1.548	66.463	57.704
	k_{id} $(g \cdot mg^{-1} \cdot h^{-0.5})$	1.783	6.960	7.854
	R^2	0.820	0.724	0.515

Table 2. Isotherm Parameters for Pb Adsorption of Ca-Modified Biochar

sample	T (K)	q_e,exp	Langmuir isotherm model				Freundlich isotherm model		
			Q_{max} $(mg \cdot g^{-1})$	K_L $(L \cdot mg^{-1})$	R_L	R^2	K_F $(mg^{1-n} \cdot g^{-1} \cdot L^{-n})$	n	R^2
CEA-1	298	19.223 ± 0.19	23.431	0.052	0.114−0.562	0.914	4.272	3.380	0.993
	318	16.075 ± 0.43	19.793	0.034	0.164−0.661	0.922	2.939	2.843	0.985
	338	13.743 ± 0.25	16.412	0.021	0.241−0.760	0.930	1.933	2.356	0.978
CEA-2	298	97.454 ± 1.26	98.811	0.218	0.029−0.234	0.987	37.742	4.752	0.898
	318	99.696 ± 1.48	102.974	0.374	0.017−0.151	0.991	41.026	5.944	0.861
	338	102.142 ± 2.16	104.249	1.138	0.006−0.055	0.994	52.248	6.896	0.789
CEA-3	298	79.967 ± 1.21	81.487	0.185	0.035−0.265	0.976	27.780	3.713	0.908
	318	83.951 ± 1.52	85.429	0.309	0.021−0.177	0.983	33.448	4.396	0.846
	338	86.392 ± 1.60	87.851	0.816	0.008−0.075	0.985	36.873	4.873	0.797

q_e and η values under a condition of 0.2 g·L^{-1}. Then, the q_e of CEA-1, CEA-2, and CEA-3 reached the maximum values (18.02, 97.74, and 83.73 mg·g^{-1}) under a condition of 0.5 g·L^{-1}, while the η values of CEA-1, CEA-2, and CEA-3 were 18.02, 97.74, and 83.73%, respectively. A large number of active sites caused by high-dose adsorbent were conducive to Pb adsorption. The η value of Ca-modified biochar continued to increase, and the q_e value began to decrease rapidly under the excessive dosage (0.5−0.7 g·L^{-1}). The active site could not be fully utilized by the agglomeration of excessive adsorbent, which inevitably reduced the unit adsorption capacity (q_e) of adsorbents.[26]

The effect of contact time on Pb adsorption of Ca-modified biochar is given in Figure 1d. When the contact time was 2 h, the q_t values of CEA-1, CEA-2, and CEA-3 were 13.16, 94.99, and 81.40 mg·g^{-1}, and they had reached 73.0, 97.1, and 97.3% of saturated adsorption capacity, respectively. The result indicated it was a fast adsorption process, which was related to the rapid diffusion of Pb species to the active sites on the adsorbent surface at the beginning of the reaction. As the reaction time increased to 8 h, the q_t values of CEA-1, CEA-2, and CEA-3 were 17.95, 97.73, and 83.68 mg·g^{-1}, and they had reached 99.6, 99.9, and 99.8% of saturated adsorption capacity, indicating a slow adsorption process. In this process, the increase of the number of positive charges on the adsorbent surface greatly hindered the continuous progress of Pb adsorption. Based on the above results, the suitable adsorption conditions of Ca-modified biochar were initial pH of 7.0, adsorbent dosage of 0.5 g L^{-1}, and contact time of 8.0 h, respectively, which were used for a subsequent adsorption experiment.

2.2. Adsorption Kinetics, Isotherms, and Thermodynamic Studies. The kinetic results of Ca-modified biochar fitted by the pseudo-first/second-order equation and intra-particle diffusion models are shown in Figure 2a−c and Table 1.

As seen in Table 1, the measured equilibrium adsorption capacity ($q_{e,exp}$) of CEA-1 is only 18.023 mg·g^{-1}, however, that of CEA-2 and CEA-3 increased to 97.742 and 83.731 mg·g^{-1}, which demonstrated only a large amount of Ca-source was helpful to increase the adsorption capacity of biochar. The fitting correlation coefficient ($R^2 = 0.976$) of pseudo-first-order of CEA-1 was higher than that ($R^2 = 0.881$) of pseudo-second-order, and the fitting q_e value (19.531 mg·g^{-1}) of first-order kinetics was closer to the $q_{e,exp}$ value (18.023 mg·g^{-1}). This result indicated that the pseudo-first-order kinetic model was more suitable to describe Pb adsorption process of CEA-1, which was mainly controlled by the diffusion process. Similarly, the Pb adsorption process of CEA-2 and CEA-3 was more consistent with the pseudo-second order model, which was mainly controlled by chemical adsorption. Especially, the pseudo-first-order of CEA-2 achieved a higher fitting accuracy ($R^2 = 0.967$) than CEA-3 ($R^2 = 0.904$), implying the important role of diffusion process on the Pb adsorption process of CEA-2.

In this case, the role of diffusion process was further confirmed by the intraparticle diffusion model.[27] As seen in Table 1, the fitting correlation coefficient (R^2) of the intraparticle diffusion model of CEA-1 could reach 0.820, and the adsorption equilibrium time of CEA-1 exceeded 8 h (Figure 1d), this result indicated the important role of intraparticle diffusion process. The driving force of this physical diffusion was the van der Waals force that belonged to the weak interaction between molecules.[28] Next, R^2 values of the intraparticle diffusion model of CEA-2 and CEA-3 were 0.742 and 0.515, respectively. This indicated that the key controlled step of CEA-3 was the interface diffusion process; however, the Pb adsorption process of CEA-2 was controlled together by intraparticle and interface diffusion. Next, the

isotherm results of Ca-modified biochar fitted by Langmuir and Freundlich isotherm models are shown in Figure 2d–f and Table 2.

As seen in Figure 2d–f, the measured equilibrium adsorption capacities (q_e) of CEA-1 decreased gradually with the increase of reaction temperature (Figure 2d), indicating an exothermic reaction. Conversely, that of CEA-2 and CEA-3 increased gradually (Figure 2e,f), indicating the endothermic reaction. Furthermore, there were significant differences in the adsorption equilibrium concentrations (C_e) of Ca-modified biochar, which was related to the key-controlled steps of the Pb adsorption process. Inyang et al.[29] found that the effect of adsorbate concentration on the chemisorption process could be almost ignored, but it played an important role in the physical adsorption of the adsorbent. Therefore, the C_e value of CEA-1 could reach 120 mg·L^{-1} during the Pb adsorption, while that of CEA-2 and CEA-3 was less than 60 mg·L^{-1}.

The Langmuir model referred to monolayer adsorption behaviors of adsorbents through chemical precipitation and hydrogen bonding, and so forth. Freundlich model meant the multilayer adsorption actions of adsorbent through Van der Waals force, and so forth.[21] As seen in Table 2, R^2 values of the Freundlich model of CEA-1 at different reaction temperatures were all higher than that of the Langmuir model, showing the multilayer adsorption characteristic. This adsorption behavior means only physical adsorption of CEA-1 through the pore structure. The Langmuir model of CEA-2 and CEA-3 had a higher fitting accuracy than the Freundlich model at the different reaction temperature, indicating monolayer adsorption behavior was the main control mode. After the addition of a lot of eggshells, the increase of active sites on the CEA-2 and CEA-3 surface could promote the formation of Ca–Pb precipitations, presenting the monolayer adsorption process.[20] In the fitting calculation of Langmuir adsorption model, the dimensionless equilibrium constant (R_L) was used to determine whether the adsorption reaction was favorable. According to the previous studies, $R_L > 1$ was unfavorable adsorption; $R_L = 1$ represented the linear adsorption, and $0 < R_L < 1$ meant the favorable adsorption.[30] As seen in Table 2, R_L values of Ca-modified biochar at the different temperatures were all less than 1, indicating the favorable adsorption process. In fitting calculation of the Freundlich adsorption model, the n value reflected the strength of adsorption reaction, and $0 < n < 10$ meant a good adsorption process.[31] The n values of Ca-modified biochar at different temperatures were between 1 and 10, indicating a good adsorption reaction between Ca-modified biochar and Pb. In addition, the K_F value was proportional to the adsorption performance of the adsorbent.[32] The K_F values of CEA-1 decreased with the increase of reaction temperature, while CEA-2 and CEA-3 had an increasing K_F value, this indicated that the high reaction temperature was only conducive to the Pb adsorption of biochar modified by a lot of eggshells. At each temperature, CEA-2 always had the higher K_F value than CEA-3, implying its stronger adsorption capacity. This conclusion could be proved from the changes of measured equilibrium adsorption capacities ($q_{e,exp}$) of CEA-2 and CEA-3 at the different temperatures.

Standard enthalpy (ΔH^0), standard entropy (ΔS^0), and Gibbs free energy (ΔG^0) of Ca-modified biochar are calculated according to eqs S1–S4.[2] According to the values of intercept and slope obtained by linear regression analysis (Figure S2), the standard enthalpy (ΔH^0), and standard entropy (ΔS^0) of

Ca-modified biochar were calculated. Gibbs free energy (ΔG^0) at different temperatures is calculated by eq S2. Thermodynamic parameters of Ca-modified biochar are shown in Table 3.

Table 3. Thermodynamic Parameters of Ca-Modified Biochar

sample	T/K	ΔG^0 (kJ·mol^{-1})	ΔH^0 (kJ·mol^{-1})	ΔS^0 (J·K^{-1}·mol^{-1})
	298	−2.50		
CEA-1	318	−1.88	−11.63	−30.65
	338	−1.26		
	298	−37.33		
CEA-2	318	−40.91	60.48	256.64
	338	−43.05		
	298	−70.07		
CEA-3	318	−72.06	35.44	219.49
	338	−74.94		

As seen in Table 3, the ΔH^0 value of CEA-1 was −11.63 kJ·mol^{-1}, indicating an exothermic reaction; thus, the adsorption capacity of CEA-1 was inhibited under the conditions of high reaction temperature. Conversely, the ΔH^0 values of CEA-2 and CEA-3 were 60.48 and 35.44 kJ·mol^{-1}, indicating an endothermic reaction; thus, the Pb adsorption capacities of CEA-2 and CEA-3 could be improved under the conditions of high reaction temperature. Then, a negative ΔS^0 value of CEA-1 indicated the enhanced order of solid solution interface during the Pb adsorption. Conversely, all positive ΔS^0 values of CEA-2 and CEA-3 showed an obvious disorder of solid–solution interface.[33] According to the previous studies,[34] the Gibbs free energy value (ΔG^0) between −20 and 0 kJ·mol^{-1} indicated a physical adsorption process and that of chemical adsorption was between −400 and −80 kJ·mol^{-1}. The ΔG^0 values of CEA-1 at the different temperatures were between −20 and 0 kJ·mol^{-1}, indicating a physical adsorption process caused by Van der Waals force or weak electrostatic interaction. The ΔG^0 values of CEA-2 and CEA-3 at different temperatures were between −80 and −20 kJ·mol^{-1}, indicating that the Pb adsorption process of CEA-2 and CEA-3 was controlled by the physical and chemical composite actions. In addition, the ΔG^0 absolute values of CEA-2 and CAE-3 gradually increased with the increase of reaction temperature from 298 to 338 K. This result proved again that elevated temperatures were conducive to improve the Pb adsorption capacities of CEA-2 and CAE-3.

2.3. Surface Morphology Analysis. Figure 3 shows the surface topography of Ca-modified biochar before adsorption and after adsorption. The CEA-1 sample had a regular, smooth, and compact surface with some pores (Figure 3a). With the gradual depolymerization of the macromolecular structure of Eupatorium adenophorum, some gaseous products (such as CO, CO_2, and C_xH_y) generated by the break of chemical bonds were rapidly released from the carbon skeleton, leading to the formation of few pores.[35] There were some fine particles dispersed on the surface of CEA-1, which might be CaO produced by the decomposition of $CaCO_3$. This result indicated that the effect of a small amount of eggshells on the surface morphology of biochar was very limited. After the addition of a lot of eggshells, the CEA-2 and CEA-3 samples had the rough and loose surface with many pores (Figure 3b,c). $CaCO_3$ could decompose into CO_2 and CaO at high temperatures (eq 4), and CO_2 could react with
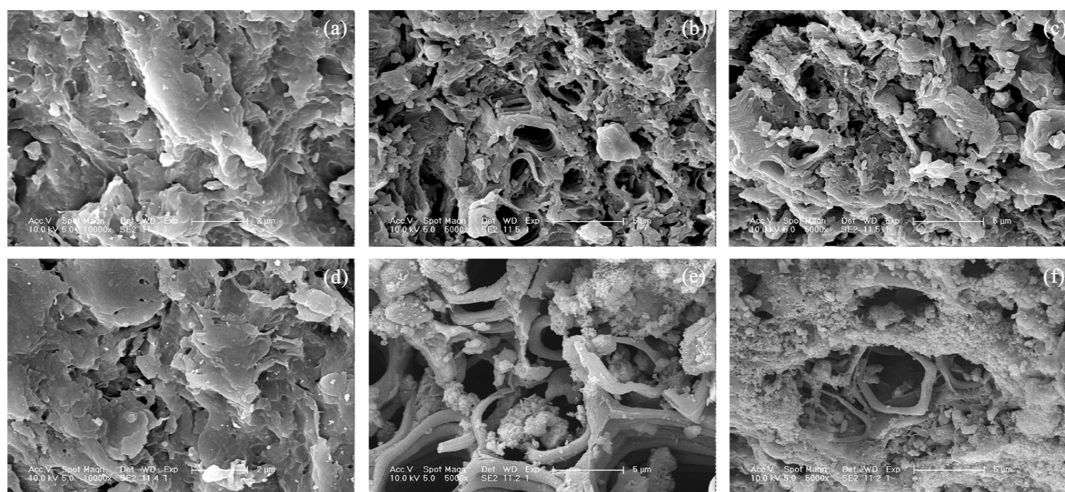
Figure 3. SEM images of Ca-modified biochar before adsorption and after adsorption (a) CEA-1; (b) CEA-2; (c) CEA-3; (d) CEA-1-Pb; (e) CEA-2-Pb; and (f) CEA-3-Pb.

the carbon matrix (eq 5) to promote the development of pore structure. However, CEA-2 had a more developed pore structure than CEA-3, which indicated that excessive eggshells might block the pore of biochar.

$$CaCO_3 \rightarrow CaO + CO_2 \qquad (4)$$

$$C + CO_2 \rightarrow 2CO \qquad (5)$$

There was almost no change for the surface morphology of CEA-1 and CEA-1-Pb before and after Pb adsorption (Figure 3a,d), and only few fine particles were observed on the surface of CEA-1-Pb. There were many crystals in micrometer size observed on the surface and internal channels of CEA-2-Pb and CEA-3-Pb (Figure 3e,f). The shape and size of these precipitates were similar to hydrocerussite [$Pb_3(CO_3)_2(OH)_2$] observed by Guo and Shi.[36] The phenomenon indicated the chemical precipitation was one of the main adsorption mechanisms of CEA-2 and CEA-3 for Pb removal. In addition, a lot of Pb precipitates could be observed within the pores and channels of CEA-2 (Figure 3e), it inferred that the developed pores of CEA-2 might make chemisorption a more adequate reaction located in pores/channels. Figure S3 shows that the O, C, and Ca elements were detected on the surface of Ca-modified biochars. After Pb adsorption, the Pb element could be detected on the surface of CEA-2-Pb and CEA-3-Pb. The result further confirmed that the chemical precipitation was the main adsorption mechanism of CEA-2 and CEA-3 for Pb removal.

2.4. Crystal Structure Analysis. Figure 4 shows the XRD patterns of Ca-modified biochar before adsorption and after adsorption. CEA-2 and CEA-3 had more obvious crystallinity than CEA-1. The obvious diffraction peaks of $Ca(OH)_2$ and CaO could be observed in the XRD pattern of CEA-2 and CEA-3, indicating the successful introduction of calcium. CaO nanoparticles derived from the thermal decomposition of $CaCO_3$ (eq 4), and the part of CaO nanoparticles reacted with H_2O to further form $Ca(OH)_2$ nanoparticles (eq 6).[37] In particular, the peak intensity of CEA-3 was higher than that of CEA-2, which was related to the addition of a lot of eggshells for the preparation of CEA-3 (the ratio of raw material to eggshell was 1:1). In addition, CEA-1 had two broad diffraction peaks (2θ = 15−30° and 2θ = 38−50°), indicating the formation of significant aromatic structure via high-
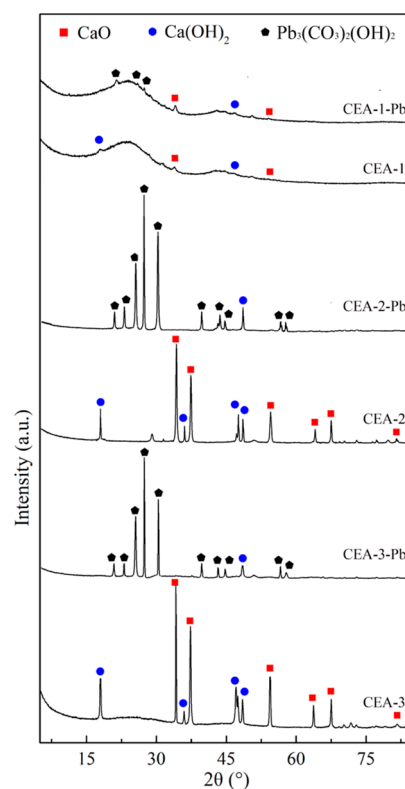

Figure 4. XRD pattern of Ca-modified biochar before adsorption and after adsorption.

temperature treatment. However, the very weak diffraction peaks of $Ca(OH)_2$ and CaO in XRD patterns of CEA-1, which might be because of the addition of very few eggshell (the ratio of raw material to eggshell was 10:1).

$$CaO + H_2O \rightarrow Ca(OH)_2 \qquad (6)$$

After the Pb adsorption experiment, the diffraction peaks of CaO and $Ca(OH)_2$ basically disappeared, and the new diffraction peaks located at 18.28, 22.37, 24.48, 27.34, 31.72, 39.63, 43.55, 45.27, 56.41, and 58.23° could be observed in the XRD pattern of CEA-2-Pb and CEA-3-Pb, which represented a kind of Pb precipitate [$Pb_3(CO_3)_2(OH)_2$].[38] These results

proved that CaO and Ca(OH)$_2$ had a strong adsorption ability for Pb and Pb$_3$(CO$_3$)$_2$(OH)$_2$ crystals were formed by the Ca−P precipitation reaction (eqs 7−9).[39] In addition, CEA-1-Pb had the weak diffraction peaks of Ca(OH)$_2$, CaO, and Pb precipitates. The kinetic and isotherm studies indicated that the Pb adsorption capacity CEA-2 and CEA-2 had the significant enhancement compared with CEA-1. In fact, the new formed precipitations also were directly found from the surface of CEA-2-Pb and CEA-3-Pb (Figure 3e,f). In addition, the crystal structures of Pb$_3$(CO$_3$)$_2$(OH)$_2$ could be confirmed again from the FTIR spectra of CEA-2-Pb and CEA-3-Pb (Figure 5).
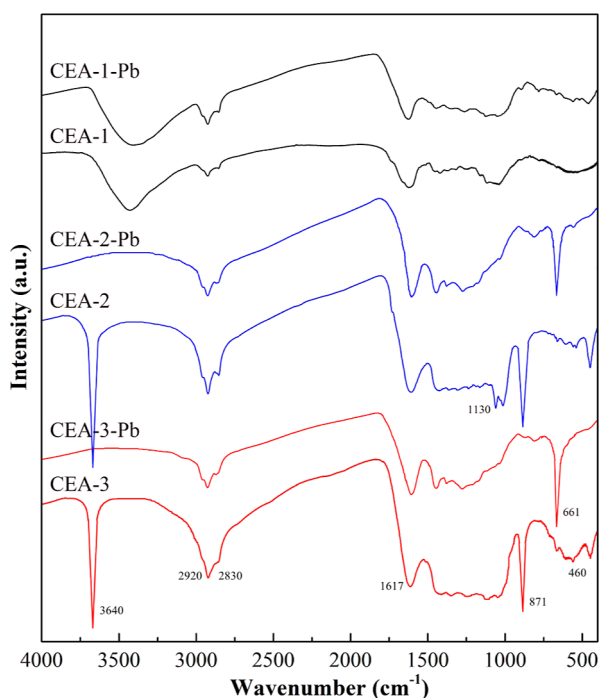
$$Pb^{2+} + 2OH^- \rightarrow Pb(OH)_2 \tag{7}$$

$$Pb^{2+} + Ca(OH)_2 \rightarrow Pb(OH)_2 + Ca^{2+} \tag{8}$$

$$3Pb(OH)_2 + 2CO_3^{2-} \rightarrow Pb_3(CO_3)(OH)_2 + 4OH^- \tag{9}$$
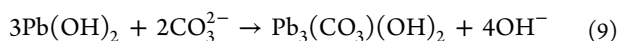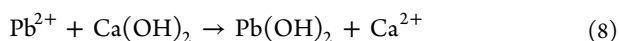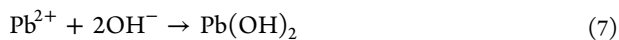

Figure 5. FTIR spectra of Ca-modified biochar before adsorption and after Pb adsorption.

2.5. Surface Chemical Group Analysis. Figure 5 shows FTIR spectra of Ca-modified biochar before adsorption and after Pb adsorption. The obvious absorption peaks at 460, 871, and 3640 cm^{-1} were observed in FTIR spectra of CEA-2 and CEA-3, which were related to the existence of Ca(OH)$_2$ and CaO.[40] This result indicated the introduction of calcium element into CEA-2 and CEA-3. Especially, CEA-2 and CEA-3 had a unique C−N stretching vibration peak at 1130 cm^{-1},[41] indicating the formation of nitrogen-containing functional groups (amides, aromatic amines, and pyridine groups). They might derive from the pyrolysis of a small amount of organic matter (about 6% protein) in eggshells. In addition, FTIR spectra of CEA-1 presented some vibration peaks at 2830 and 2920, 1617, and 750−810 cm^{-1}. According to previous studies,[2,42] 2830 and 2920 cm^{-1} belonged to the stretching vibration of the aliphatic C−H bond; the stretching vibration

peaks of the aromatic C═C bond located at 1617 cm^{-1}; and the deformed vibration peaks of aromatic C−H bond located at 750−810 cm^{-1}. FTIR spectra of CEA-1 indicated that the formation of only some stable aromatic structure via high-temperature treatment. This result confirmed that the addition of few eggshells (the ratio of raw material to eggshell was 10:1) could not effectively modify biochar.

After the Pb adsorption experiment, FTIR spectra of CEA-1-Pb was similar to that of CEA-1, indicating almost no Pb precipitates on the surface of CEA-1-Pb. This result suggested that chemical adsorption might not be the Pb adsorption mechanism of CEA-1. The disappeared absorption peaks of Ca(OH)$_2$ and CaO and a new absorption peak at 661 cm^{-1} referred to Pb$_3$(CO$_3$)$_2$(OH)$_2$ were observed on the surface of CEA-2-Pb and CEA-3-Pb.[43] In particular, the CEA-3-Pb had the higher absorption peak of Pb$_3$(CO$_3$)$_2$(OH)$_2$ than CEA-2-Pb, indicating the strong precipitation reaction on the surface of CEA-3. In addition, the disappearance of the C−N stretching vibration peak in CEA-2-Pb and CEA-3-Pb confirmed that nitrogen-containing functional groups interacted with Pb^{2+}, which enhanced the affinity of CEA-2 and CEA-3 for heavy metal ions. Shang et al.[44] studied the Pb^{2+} adsorption performance of corncob xylose residue biochar. They also observed the disappearance of the C−N stretching vibration peak after the adsorption experiment, which further confirmed the complex coordination reaction (eq 10). The above results demonstrated that the chemical precipitation and complex coordination were the main adsorption mechanism of CEA-2 and CEA-3.

$$Pb^{2+} + R-NH \rightarrow R-NPb^+ \tag{10}$$
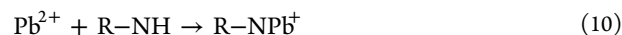
2.6. Pore Structure Analysis. Table 4 shows the pore parameter of Ca-modified biochar before and after Pb adsorption. The BET surface area, pore volume, and average pore diameter of CEA-1 were 67 m^2·g^{-1}, 0.06 cm^3·g^{-1}, and 1.74 nm, respectively, indicating the low porosity. This might be due to the fact that a small amount of eggshells could not effectively decompose of tar components produced during pyrolysis. Then, the BET surface area, pore volume, and average pore diameter of CEA-2 were 621 m^2·g^{-1}, 0.38 cm^3·g^{-1}, and 2.37 nm, respectively, indicating the developed pore structure. During high-temperature treatment, CaCO$_3$ could decompose into CO$_2$ and CaO, in which CO$_2$ could react with the carbon matrix to remove the carbon impurities (including tar and inorganic debris) within the pores and channels.[45] However, the BET surface area, pore volume, and average pore diameter of CEA-3 rapidly decreased under the addition of
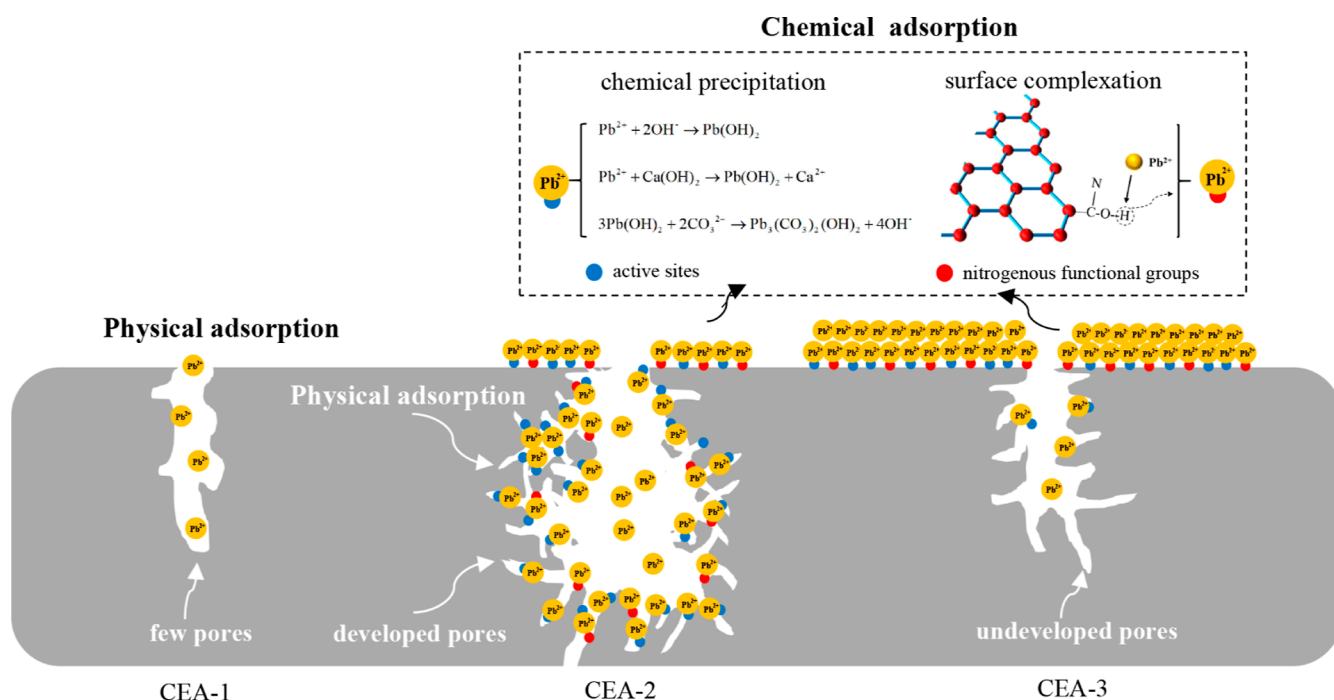
Table 4. Pore Parameter of Ca-Modified Biochar Before and After Pb Adsorption[a]

sample	S_{BET} (m^2·g^{-1})	V_t (cm^3·g^{-1})	V_{mic} (cm^3·g^{-1})	$V_{non-mic}$ (cm^3·g^{-1})	D_{ap} (nm)
CEA-1	67	0.06	0.04	0.02	1.74
CEA-2	621	0.38	0.22	0.16	2.37
CEA-3	269	0.19	0.11	0.08	1.82
CEA-1-Pb	63	0.05	0.03	0.02	1.72
CEA-2-Pb	155	0.10	0.06	0.04	1.93
CEA-3-Pb	214	0.15	0.08	0.07	2.07

^{a}S_{BET}: specific surface area; V_t: total pore volume; V_{mic}: micropore volume; $V_{non-mic}$: mesopores and macropores volume; and D_{ap}: average pore diameters.

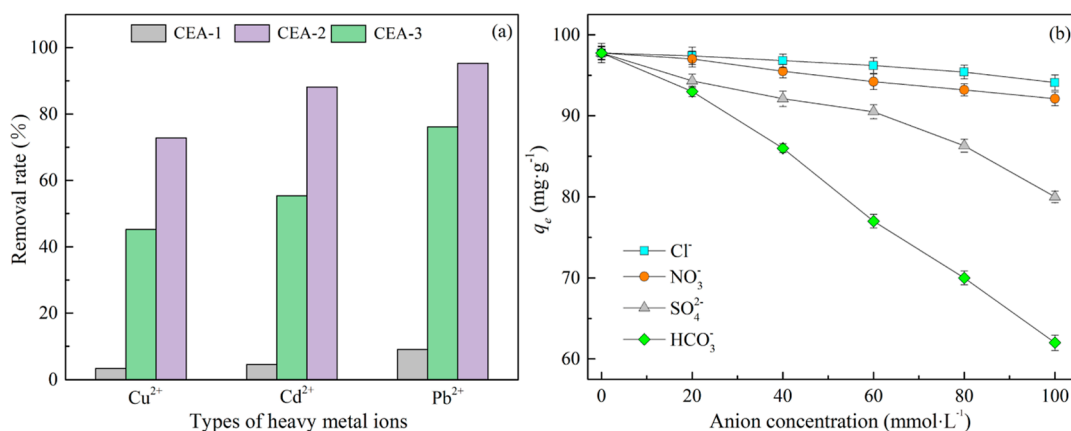**Figure 6.** Pb adsorption mechanism of Ca-modified biochar.

Figure 7. Adsorption performance of Ca-modified biochar in a ternary heavy metal system (a), and influence of coexisting anions on Pb adsorption of CEA-2 (b).

excessive eggshells. The excessive catalysts could agglomerate with each other during the pyrolysis, it was difficult to give full play to their catalytic cracking characteristics, resulting in the undeveloped pore structure.

After the Pb adsorption experiment, the pore parameters of CEA-1-Pb had no obvious changes. The BET surface area, pore volume, and average pore diameter of CEA-2-Pb decreased significantly to 155 $m^2 \cdot g^{-1}$, 0.1 $cm^3 \cdot g^{-1}$, and 1.93 nm. In the adsorption process, Pb could combine with active sites located inside the pore/channel to form many Pb precipitations, which could block the pores. In addition, a lot of precipitates within the pores and channels of CEA-2 also could be directly observed in Figure 3e. Next, BET surface area, pore volume, and average pore diameter of CEA-3-Pb decreased slightly. This result indicated that undeveloped pores made it difficult for Pb to diffuse smoothly into CEA-3. Therefore, the formation of Pb precipitation was mainly on the surface of CEA-3-Pb rather than its interior, which was not

conducive to the continuous adsorption. Such a phenomenon could also be observed in Figure 3f.

Figure 6 shows the Pb adsorption mechanism of Ca-modified biochar. CEA-1 almost no functional groups and Ca-based active sites. Only a small amount of Pb could be adsorbed by the undeveloped pores of CEA-1. Therefore, the physical adsorption was the main controlled step of CEA-1 for the Pb removal. CEA-2 and CEA-3 had many Ca-based active sites and abundant nitrogenous functional groups, which were conducive to Pb removal through the precipitate reaction and surface complexation. Significantly, the developed pore of CEA-2 helped to the diffusion of Pb into the interior of the particles, which ensured the full utilization of active sites within the pores/channels to achieve continuous adsorption. However, the undeveloped pore of CEA-3 allowed chemical adsorption to take place more on the particle surface rather than the interior. In addition, CEA-2 had a higher Pb adsorption capacity of 97.74 $mg \cdot g^{-1}$ than the other biosorbents produced from eggshells (90.9 $mg \cdot g^{-1}$),[46] chitosan (71 mg·
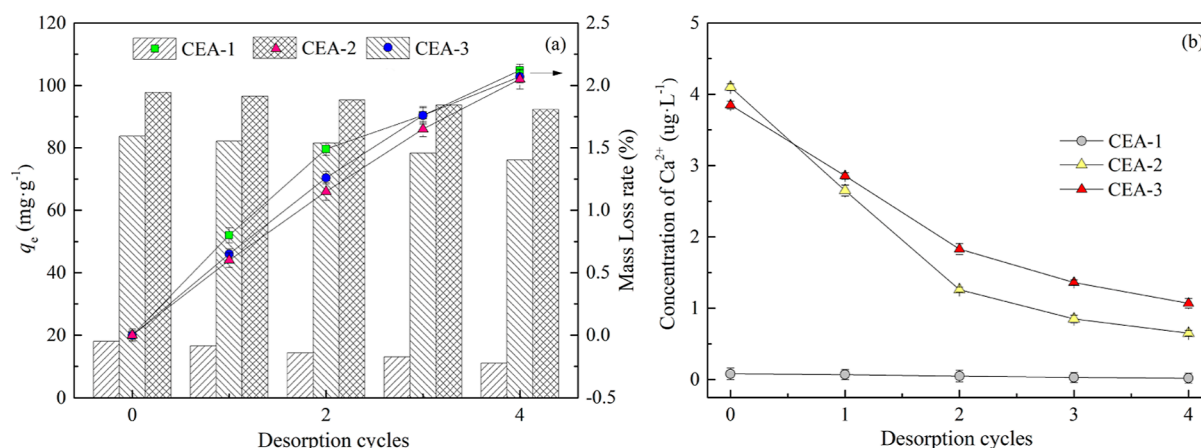
Figure 8. Adsorption capacity and mass loss (a) and Ca^{2+} concentration (b) of Ca-modified biochar under four desorption cycles.

g^{-1}),[47] and sugarcane bagasse (21 mg·g^{-1})[48] in the previous literature. The results from this paper proved the feasibility of waste eggshells as a Ca-source could produce the cheap and efficient biochar adsorbent for heavy metal adsorption from the wastewater.

2.7. Influence of Coexisting Cations and Anions. Often in wastewater streams, besides Pb, other heavy metals were present. The ternary heavy metal system, including Cu, Cd, and Pb, was used to explore the actual adsorption performance of Ca-modified biochar. The initial concentrations of Cu, Cd, and Pb in the mixed solution were 50 mg·L^{-1}, and the dosage of Ca-modified biochar was 0.5 g·L^{-1}. This experiment was performed at 298 K and 120 rpm for 8.0 h. As seen in Figure 7a, the CEA-2 sample had the highest removal rate of heavy metals (Cu^{2+}: 72.75%, Cd^{2+}: 88.12%, and Pb^{2+}: 95.31%) among the three samples, and the CEA-1 sample had the lowest removal rate (Cu^{2+}: 3.32%, Cd^{2+}: 4.51%, and Pb^{2+}: 9.04%). In addition, the removal rate of the CEA-3 sample was between CEA-1 and CEA-2. This result indicated that CEA-2 had the prominent adsorption performance for a variety of heavy metals. Significantly, the Pb removal rate of each sample in the ternary heavy metal system was lower than that in a separate Pb solution. This result proved that Cu and Cd could compete with Pb for adsorption sites in the mixed solution.

In addition to above cations, NO_3^-, HCO_3^-, SO_4^{2-}, and Cl^- were also common anions in wastewater, these anions could affect the Pb adsorption performance of adsorbents. CEA-2 had the highest adsorption performance among three kinds of Ca-modified biochar; thus, the effect of coexisting anions on Pb adsorption of CEA-2 is investigated in Figure 7b. As seen in Figure 7b, the adsorption performance of CEA-2 was inhibited by these anions at different levels, following the order of $HCO_3^- > SO_4^{2-} > NO_3^- > Cl^-$. Among these ions, NO_3^- and Cl^- had a very limited impact on the Pb adsorption performance of CEA-2. Even if the ion concentration of NO_3^- and Cl^- reached 100 mmol·L^{-1}, the adsorption capacity of CEA-2 could still maintain a high adsorption capacity (NO_3^-: 94.2 mg·g^{-1} and Cl^-: 92.5 mg·g^{-1}). However, HCO_3^- and SO_4^{2-} had a very significant inhibitory effect on the Pb adsorption performance of CEA-2. With the increase of ion concentration (~100 mmol·L^{-1}), the adsorption capacity of CEA-2 decreased significantly. When the ion concentration of HCO_3^- and SO_4^{2-} was 100 mmol·L^{-1}, the adsorption capacity of CEA-2 reached only 80.1% (SO_4^{2-}) and 61.6% (HCO_3^-), respectively. In this process, HCO_3^- and SO_4^{2-} could combine

with Ca^{2+} to produce insoluble substances or poorly soluble substances, resulting in the reduction of active sites on the surface of the adsorbent.

2.8. Regeneration Test. In practical applications, desorption regeneration, mass loss, and release of calcium ions of Ca-modified biochar are very important factors. As seen in Figure 8a, the Pb adsorption capacity of Ca-modified biochar decreased gradually with the increase of cycle number. Although the adsorption capacity of CEA-2 decreased from 97.742 to 92.32 mg·g^{-1} after four desorption cycles, but it still had the highest adsorption capacity than CAE-1 and CEA-3. This result indicated that the CEA-2 sample had good recycling performance in the treatment of wastewater containing Pb. In addition, the mass loss rate of Ca-modified biochar increased slightly during the cyclic degradation. However, there was no obvious difference in the mass loss rate of the three samples (2.05−2.12%). Finally, the inductively coupled plasma (ICP, ICPE-9000, Shimadzu, Japan) was used to determine the Ca^{2+} concentration of the solution. As seen in Figure 8b, the Ca^{2+} concentration of CEA-1 was almost 0 during cyclic degradation, which was related to the addition of few eggshells (the ratio of raw material to eggshell was 10:1). However, the Ca^{2+} concentration of CEA-2 and CEA-3 decreased gradually with the increase of cycle number, and the Ca^{2+} concentration of CEA-3 was always higher than CEA-2, which was related to the addition of excessive eggshells. However more importantly, they always had the very low concentration (~4.1 μg·L^{-1}) of calcium during the cyclic degradation, this result indicated that almost all of Ca-based active sites in CEA-2 and CEA-3 were used for the Pb adsorption rather than being released into the solution. In addition, Ca was the environmentally friendly element with non-toxic properties. Therefore, the CEA-2 sample had the best reusability among the three samples for Pb adsorption.

3. CONCLUSIONS

In this work, Ca-modified biochar adsorbents (CEA) were prepared by the pyrolysis of Eupatorium adenophorum and eggshell for the Pb adsorption from aqueous solution. CEA-2 and CEA-3 showed excellent adsorption performance with the equilibrium adsorption amounts of 97.74 and 83.73 mg·g^{-1}, respectively. The Pb adsorption process of CEA-2 and CEA-3 exhibited the monolayer adsorption, which was mainly controlled by chemical adsorption. CEA-2 and CEA-3 had many Ca-based active sites and abundant nitrogenous

functional groups, which were conducive to Pb removal through the precipitate reaction and surface complexation. Significantly, the developed pores of CEA-2 improved the contact probability between Pb and active sites within the pores and channels, which ensured continuous adsorption. In addition, the Pb adsorption process of CEA-1 exhibited the multilayer adsorption characteristics, which was mainly controlled by physical adsorption. The application experiment indicated that CEA-2 had the best cycle stability and reusability among the three samples. This research provided an effective method to prepare cheap adsorbents for Pb adsorption, which was beneficial to the wide application of biochar.

4. EXPERIMENTAL SECTION

4.1. Preparation of Ca-Modified Biochar. Eupatorium adenophorum was used as a raw material of biochar because of its high carbon content, strong renewability, and large resources. Eupatorium adenophorum was collected from a village in Chongqing city, China, which was air-dried, chopped, and sieved through 100 meshes before the experiment. Table 5

Table 5. Proximate and Ultimate Analyses of Eupatorium Adenophorum

proximate analysis (wt %)	
moisture[a]	5.07 ± 0.34
ash[b]	6.71 ± 0.11
organics[c]	88.22 ± 0.45
elemental analysis (wt %)[d]	
C	42.37
H	6.25
O[e]	42.60
N	2.07
H/C $(mol \cdot mol^{-1})$	1.77
O/C $(mol \cdot mol^{-1})$	0.75

[a]Determined by drying in an oven at 105 °C for 12 h. [b]Determined by combusting the pre-dried cornstalk in a muffle furnace at 575 °C for at least 3 h until a constant weight. [c]Determined by difference. [d]On a dry basis. [e]Determined by difference (100% − C % − H % − N % − ash %).

shows the proximate and elemental analyses of Eupatorium adenophorum. Eggshell as a calcium-source was collected from the canteen of Jilin agricultural university, which was dried, grounded, and sieved through 200 meshes before use. Next, the preparation process of Ca-modified biochar adsorbent was as follows. 20 g of Eupatorium adenophorum (marked as EA) and the eggshell with different weights (2, 10, or 20 g) were fully mixed in the ball mill (PULVERISETTE 5, FRITSCH, Germany) for 40 min. Because the complete decomposition temperature of $CaCO_3$ was 800 °C; thus the mixture was placed in a tubular furnace (OTF-1200X-III-S, Kejing, China), heated up to 800 °C at 8 °C/min under a N_2 atmosphere, and then was kept at 800 °C for 1.5 h. Ca-modified biochar with the mass ratios of eggshell to raw material of 1:10, 1:2, and 1:1 was marked as CEA-1, CEA-2, and CEA-3, respectively.

4.2. Experimental Procedures. The solution used in the experiment was prepared with ultrapure water, and all the experiments were repeated at least three times to avoid the error. Batch adsorption experiment: Ca-modified biochar with different doses $(0.2-0.8 \text{ g} \cdot L^{-1})$ was mixed into 50 mL of Pb solution with a concentration of 50 mg·L^{-1}. The initial pH

value of the mixture was set to 2.0, 3.0, 4.0, 5.0, 6.0, 7.0, and 8.0, respectively. This reaction system was stirred at 100 rpm for 12 h. Finally, the Pb concentration of reaction system was measured by an atomic absorption spectrophotometer with a detection limit of 0.0092 μg·mL^{-1} (iCE 3300 AAS, Thermo Scientific, USA), and the equilibrium adsorption capacity and the pollutant removal rate are calculated by eqs 11 and 12.

$$q_e = [(C_0 - C_e)V]/m \tag{11}$$

$$\eta = [(C_0 - C_e)/C_0] \times 100\% \tag{12}$$

where q_e is the equilibrium adsorption capacity $(mg \cdot g^{-1})$; m presents the mass of adsorbent (g); V presents the volume of solution (L); C_0 is the initial concentration of solution (mg·L^{-1}); C_e is the residual concentration of solution (mg·L^{-1}); and η presents the pollutant removal rate (%).

Desorption regeneration experiment: the saturated biochar was taken out from the reaction solution, then was repeatedly washed with ultrapure water to neutral. The washed biochar was mixed fully with EDTA solution (0.01 mol·L^{-1}) for the desorption experiment. Finally, the Pb adsorption experiment was continued with the desorbed biochar. Such an adsorption/desorption experiment was carried out four times.

Adsorption kinetics experiment: Ca-modified biochar with 0.5 g·L^{-1} was mixed into 50 mL of Pb solution with a concentration of 50 mg·L^{-1}. The initial pH value of reaction system was set to 7.0 ± 0.05. Then, this reaction system was oscillated at 298 K for different times (0.083, 0.16, 0.32, 0.5, 1, 2, 4, 6, 8, 12, 18, and 24 h). Pseudo-first/second-order models and intragranular diffusion model were used for kinetics analysis, and the corresponding definition is given in eqs S5−S7.[2]

Adsorption isotherm experiment: Ca-modified biochar with 0.5 g·L^{-1} was mixed into 50 mL of Pb solution with different concentrations of 15, 25, 40, 60, 80, 100, 120, and 150 mg·L^{-1}. The initial pH value of reaction system was set to 7.0 ± 0.05. Then, this reaction system was oscillated at different temperatures (298, 318, and 338 K) for 8 h. Langmuir and Freundlich models were used for isotherms analysis, and the definition of two models are given in eqs S8−S10.[2]

4.3. Product Analysis. Proximate analysis of raw material was calculated according to GB/T212-2008 standards. The carbon (C), hydrogen (H), and nitrogen (N) elementals in raw materials were defined using an elemental analyzer (FlashSmart, Thermo Scientific, USA), and the oxygen content was obtained by the subtraction method (100% − C % − H % − N % − ash %). Crystal structure was determined by XRD (XRD-7000, Shimadzu, Japan) with a scanning rate of 10°/min in the range of 10−80°. Surface morphology was determined by SEM (VOLUMESCOPE 2, Thermo Scientific, USA). Fourier transform infrared spectroscopy (IFS 66v/s, Bruker, Germany) provided the detailed information about the functional groups on the surface of samples. The BET nitrogen adsorption instrument (ASAP2020, Micromeritics, USA) was used to test the pore parameters of sample at 77 K, and the specific surface area, micropore volume, and total pore volume were calculated according to the BET model, t-plot method, Horvath−Kawazoe (HK), and the density functional theory (NLDFT).[49,50] Before the test, each sample was degassed under vacuum at 473 K for 10 h.

ASSOCIATED CONTENT

Ⓢ Supporting Information

The Supporting Information is available free of charge at https://pubs.acs.org/doi/10.1021/acsomega.2c01957.

Plot of determination of pH_{PZC} of Ca-modified biochar, linear plot of $\ln K^0$ versus $1/T$ for Pb adsorption on Ca-modified biochar at different temperatures, EDS elemental mapping images of Ca-modified biochar before and after adsorption, equations of standard enthalpy (ΔH^0), standard entropy (ΔS^0), and Gibbs free energy (ΔG^0) of Ca-modified biochar, equations of pseudo-first-/-second-order models and intragranular diffusion model of Ca-modified biochar, and equations of Langmuir and Freundlich models of Ca-modified biochar (PDF)

AUTHOR INFORMATION

Corresponding Author

Hongfu Ai − *College of Information Technology, Jilin Agricultural University, Changchun 130118, P. R. China;* Ⓞorcid.org/0000-0002-6113-8543; Email: jlauhongfuai@163.com

Authors

Dongdong Liu − *Key Laboratory of Straw Biology and Utilization, The Ministry of Education, Jilin Agricultural University, Changchun 130118, P. R. China; College of Engineering and Technology, Jilin Agricultural University, Changchun 130118, P. R. China;* Ⓞorcid.org/0000-0003-4789-7663

Zhengkai Hao − *College of Engineering and Technology, Jilin Agricultural University, Changchun 130118, P. R. China*

Dengqian Chen − *College of Engineering and Technology, Jilin Agricultural University, Changchun 130118, P. R. China*

Lipeng Jiang − *College of Engineering and Technology, Jilin Agricultural University, Changchun 130118, P. R. China*

Tianqi Li − *College of Engineering and Technology, Jilin Agricultural University, Changchun 130118, P. R. China*

Bing Tian − *College of Engineering and Technology, Jilin Agricultural University, Changchun 130118, P. R. China*

Cuiping Yan − *College of Engineering and Technology, Jilin Agricultural University, Changchun 130118, P. R. China*

Yuan Luo − *College of Engineering and Technology, Jilin Agricultural University, Changchun 130118, P. R. China*

Guang Chen − *Key Laboratory of Straw Biology and Utilization, The Ministry of Education, Jilin Agricultural University, Changchun 130118, P. R. China;* Ⓞorcid.org/0000-0003-4413-2358

Complete contact information is available at:
https://pubs.acs.org/10.1021/acsomega.2c01957

Author Contributions

The manuscript was written through contributions of all authors. All authors have given approval to the final version of the manuscript.

Notes

The authors declare no competing financial interest.

ACKNOWLEDGMENTS

REFERENCES

(1) Han, Y.; Boateng, A. A.; Qi, P. X.; Lima, I. M.; Chang, J. Heavy metal and phenol adsorptive properties of biochars from pyrolyzed switchgrass and woody biomass in correlation with surface properties. *J. Environ. Manage.* **2013**, *118*, 196−204.

(2) Liu, D.; Tang, Y.; Li, J.; Hao, Z.; Zhu, J.; Wei, J.; Liu, C.; Dong, L.; Jia, B.; Chen, G. Eupatorium adenophorum derived adsorbent by hydrothermal-assisted HNO_3 modification and application to Pb^{2+} adsorption. *J. Environ. Chem. Eng.* **2021**, *9*, 105972.

(3) Naeem, I.; Masood, N.; Turan, V.; Iqbal, M. Prospective usage of magnesium potassium phosphate cement combined with Bougainvillea alba derived biochar to reduce Pb bioavailability in soil and its uptake by Spinacia oleracea L. *Ecotoxicol. Environ. Saf.* **2021**, *208*, 111723.

(4) Turan, V. Potential of pistachio shell biochar and dicalcium phosphate combination to reduce Pb speciation in spinach, improved soil enzymatic activities, plant nutritional quality, and antioxidant defense system. *Chemosphere* **2021**, *245*, 125611.

(5) Khan, M. A.; Mahmood-ur-Rahman; Ramzani, P. M. A.; Zubair, M.; Rasool, B.; Khan, M. K.; Ahmed, A.; Khan, S. A.; Turan, V.; Iqbal, M. Associative effects of lignin-derived biochar and arbuscular mycorrhizal fungi applied to soil polluted from Pb-acid batteries effluents on barley grain safety. *Sci. Total Environ.* **2020**, *710*, 136294.

(6) Turan, V. Confident performance of chitosan and pistachio shell biochar on reducing Ni bioavailability in soil and plant plus improved the soil enzymatic activities, antioxidant defense system and nutritional quality of lettuce. *Ecotoxicol. Environ. Saf.* **2019**, *183*, 109594.

(7) Turan, V.; Ramzani, P. M. A.; Ali, Q.; Abbas, F.; Iqbal, M.; Irum, A.; Khan, W.-u. -D. Alleviation of nickel toxicity and an improvement in zinc bioavailability in sunflower seed with chitosan and biochar application in pH adjusted nickel contaminated soil. *Arch. Agron. Soil Sci.* **2018**, *64*, 1053−1067.

(8) Shahbaz, A. K.; Adnan Ramzani, P. M.; Saeed, R.; Turan, V.; Iqbal, M.; Lewińska, K.; Abbas, F.; Saqib, M.; Tauqeer, H. M.; Iqbal, M.; Fatima, M.; Rahman, M.-u. Effects of biochar and zeolite soil amendments with foliar proline spray on nickel immobilization, nutritional quality and nickel concentrations in wheat. *Ecotoxicol. Environ. Saf.* **2019**, *173*, 182−191.

(9) Zubair, M.; Adnan Ramzani, P. M.; Rasool, B.; Khan, M. A.; ur-Rahman, M.; Akhtar, I.; Turan, V.; Tauqeer, H. M.; Farhad, M.; Khan, S. A.; Iqbal, J.; Iqbal, M. Efficacy of chitosan-coated textile waste biochar applied to Cd-polluted soil for reducing Cd mobility in soil and its distribution in moringa (Moringa oleifera L.). *J. Environ. Manage.* **2021**, *284*, 112047.

(10) Turan, V.; Khan, S. A.; Mahmood-ur-Rahman; Iqbal, M.; Ramzani, P. M. A.; Fatima, M. Promoting the productivity and quality of brinjal aligned with heavy metals immobilization in a wastewater irrigated heavy metal polluted soil with biochar and chitosan. *Ecotoxicol. Environ. Saf.* **2018**, *161*, 409−419.

(11) Liu, D.; Jia, B.; Liu, X.; Zhao, B.; Gao, J.; Cao, Q.; Wu, S.; Qin, Y. Effects of oxygen functional groups and $FeCl_3$ on the evolution of physico-chemical structure in activated carbon obtained from Jixi bituminous coal. *RSC Adv.* **2018**, *8*, 8569−8579.

(12) Zhou, Q.; Jiang, X.; Guo, Y.; Zhang, G.; Jiang, W. An ultra-high surface area mesoporous carbon prepared by a novel MnO-templated method for highly effective adsorption of methylene blue. *Chemosphere* **2018**, *201*, 519−529.

(13) Ihsanullah, A. A.; Abbas, A.; Al-Amer, A. M.; Laoui, T.; Al-Marri, M. J.; Nasser, M. S.; Khraisheh, M.; Atieh, M. A. Heavy metal removal from aqueous solution by advanced carbon nanotubes: Critical review of adsorption applications. *Sep. Purif. Technol.* **2016**, *157*, 141−161.

(14) Dong, L. J.; Li, J. M.; Zhao, B. J.; Wang, Y. T.; Chen, G.; Liu, D. D. Structure characterization and Pb^{2+} adsorption mechanism of nitric acid modified hydrochars from straw. *Trans. Chin. Soc. Agric. Mach.* **2013**, *52*, 267−278.

(15) Mahdavi, S.; Jalali, M.; Afkhami, A. Removal of heavy metals from aqueous solutions using Fe3O4, ZnO, and CuO nanoparticles. *J. Nanopart. Res.* **2012**, *14*, 846.

(16) Li, R.; Wang, J. J.; Zhou, B.; Zhang, Z.; Liu, S.; Lei, S.; Xiao, R. Simultaneous capture removal of phosphate, ammonium and organic substances by MgO impregnated biochar and its potential use in swine wastewater treatment. *J. Cleaner Prod.* **2017**, *147*, 96−107.

(17) Khairol, N. F.; Sapawe, N.; Danish, M. Study of the optical properties of zinc incorporated onto eggshell using UV-vis diffuse reflectance spectroscopy. *Mater. Today: Proc.* **2020**, *31*, 245−248.

(18) Khairol, N. F.; Sapawe, N.; Danish, M. Tailoring the optical properties of zinc/copper−incorporated onto eggshell synthesized via electrochemical method. *Mater. Today: Proc.* **2020**, *31*, 241−244.

(19) Fahmi Khairol, N.; Sapawe, N.; Danish, M. Effective Photocatalytic Removal of Different Dye Stuffs Using ZnO/CuO-Incorporated onto Eggshell Templating. *Mater. Today: Proc.* **2019**, *19*, 1255−1260.

(20) Mitrogiannis, D.; Psychoyou, M.; Baziotis, I.; Inglezakis, V. J.; Koukouzas, N.; Tsoukalas, N.; Palles, D.; Kamitsos, E.; Oikonomou, G.; Markou, G. Removal of phosphate from aqueous solutions by adsorption onto $Ca(OH)_2$ treated natural clinoptilolite. *Chem. Eng. J.* **2017**, *320*, 510−522.

(21) Wang, S.; Kong, L.; Long, J.; Su, M.; Diao, Z.; Chang, X.; Chen, D.; Song, G.; Shih, K. Adsorption of phosphorus by calcium-flour biochar: isotherm, kinetic and transformation studies. *Chemosphere* **2018**, *195*, 666−672.

(22) Quina, M. J.; Soares, M. A. R.; Quinta-Ferreira, R. Applications of industrial eggshell as a valuable anthropogenic resource. *Resour., Conserv. Recycl.* **2017**, *123*, 176−186.

(23) Cheng, S.; Zhang, L.; Xia, H.; Zhang, S.; Peng, J.; Wang, S. Crofton weed derived activated carbon by microwave-induced KOH activation and application to wastewater treatment. *J. Porous Mater.* **2016**, *23*, 1597−1607.

(24) Bogusz, A.; Oleszczuk, P.; Dobrowolski, R. Application of laboratory prepared and commercially available biochars to adsorption of cadmi-um, copper and zinc ions from water. *Bioresour. Technol.* **2015**, *196*, 540−549.

(25) Wang, G.; Zhang, S.; Yao, P.; Chen, Y.; Xu, X.; Li, T.; Gong, G. Removal of Pb(II) from aqueous solutions by Phytolacca americana L. biomass as a low cost biosorbent. *Arabian J. Chem.* **2018**, *11*, 99−110.

(26) Ahmad, M.; Rajapaksha, A. U.; Lim, J. E.; Ming, Z.; Bolan, N.; Mohan, D.; Vithanage, M.; Sang, S. L.; Yong, S. O. Biochar as a sorbent for contaminant management in soil and water: a review. *Chemosphere* **2014**, *99*, 19−33.

(27) Iida, T.; Amano, Y.; Machida, M.; Imazeki, F. Effect of surface property of activated carbon on adsorption of nitrate ion. *Chem. Pharm. Bull.* **2013**, *61*, 1173−1177.

(28) Ahmad, M.; Hashimoto, Y.; Moon, D. H.; Lee, S. S.; Ok, Y. S. Immobilization of lead in a korean military shooting range soil using eggshell waste. *J. Hazard. Mater.* **2012**, *209−210*, 392−401.

(29) Inyang, M.; Gao, B.; Pullammanappallil, P.; Ding, W.; Zimmerman, A. R. Biochar from anaerobically digested sugarcane bagasse. *Bioresour. Technol.* **2010**, *101*, 8868−8872.

(30) Papandreou, A.; Stournaras, C. J.; Panias, D. Copper and cadmium adsorption on pellets made from fired coal fly ash. *J. Hazard. Mater.* **2007**, *148*, 538−547.

(31) Milojkovic, J. V.; Mihajlovic, M. L.; Stojanovic, M. D.; Lopičić, Z. R.; Petrović, M. S.; Sostaric, T.; Ristić, M. . Đ. Pb(II) removal from aqueous solution by Myriophyllum spicatum and its compost: equilibrium, kinetic and thermodynamic study. *J. Chem. Technol. Biotechnol.* **2014**, *89*, 662−670.

(32) Jia, Y. F.; Thomas, K. M. Adsorption of cadmium ions on oxygen surface sites in activated carbon. *Langmuir* **2000**, *16*, 1114−1122.

(33) Anastopoulos, I.; Massas, I.; Ehaliotis, C. Composting improves biosorption of Pb^{2+} and Ni^{2+} by renewable lignocellulosic materials. Characteristics and mechanisms involved. *Chem. Eng. J.* **2013**, *231*, 245−254.

(34) Liu, Q.-S.; Zheng, T.; Wang, P.; Jiang, J.-P.; Li, N. Adsorption isotherm, kinetic and mechanism studies of some substituted phenols on activated carbon fibers. *Chem. Eng. J.* **2010**, *157*, 348−356.

(35) Zhai, Y.; Liu, X.; Zhu, Y.; Peng, C.; Wang, T.; Zhu, L.; Li, C.; Zeng, G. Hydrothermal carbonization of sewage sludge: The effect of feed-water pH on fate and risk of heavy metals in hydrochars. *Bioresour. Technol.* **2016**, *218*, 183−188.

(36) Guo, X.; Shi, H. Microstructure and heavy metal adsorption mechanisms of hydrothermally synthesized Al-substituted tobermorite. *Mater. Struct.* **2017**, *50*, 245.

(37) Ma, J.; Qi, J.; Yao, C.; Cui, B.; Zhang, T.; Li, D. A novel bentonite-based adsorbent for anionic pollutant removal from water. *Chem. Eng. J.* **2012**, *200−202*, 97−103.

(38) De Velasco Maldonado, P. S.; Hernández-Montoya, V.; Concheso, A.; Montes-Morán, M. A. Formation of cerussite and hydrocerussite during adsorption of lead from aqueous solution on oxidized carbons by cold oxygen plasma. *Appl. Surf. Sci.* **2016**, *386*, 381−388.

(39) Inyang, M. I.; Gao, B.; Yao, Y.; Xue, Y.; Zimmerman, A.; Mosa, A.; Pullammanappallil, P.; Ok, Y. S.; Cao, X. A review of biochar as a low-cost adsorbent for aqueous heavy metal removal. *Crit. Rev. Environ. Sci. Technol.* **2016**, *46*, 406−433.

(40) Peng, C.; Zhai, Y.; Zhu, Y.; Xu, B.; Wang, T.; Li, C.; Zeng, G. Production of char from sewage sludge employing hydrothermal carbonization: Char properties, combustion behavior and thermal characteristics. *Fuel* **2016**, *176*, 110−118.

(41) Meng, F.; Yu, J.; Tahmasebi, A.; Han, Y.; Zhao, H.; Lucas, J.; Wall, T. Characteristics of chars from low-temperature pyrolysis of lignite. *Energy Fuels* **2013**, *28*, 275−284.

(42) Liew, R. K.; Nam, W. L.; Chong, M. Y.; Phang, X. Y.; Su, M. H.; Yek, P. N. Y.; Ma, N. L.; Cheng, C. K.; Chong, C. T.; Lam, S. S. Oil palm waste: An abundant and promising feedstock for microwave pyrolysis conversion into good quality biochar with potential multi-applications. *Process Saf. Environ.* **2018**, *115*, 57−69.

(43) Kong, L.; Han, M.; Shih, K.; Su, M.; Diao, Z.; Long, J.; Chen, D.; Hou, L. a.; Peng, Y. Nano-rod Ca-decorated sludge derived carbon for removal of phosphorus. *Environ. Pollut.* **2018**, *233*, 698−705.

(44) Shang, H.; Li, Y.; Liu, J.; Wan, Y.; Feng, Y.; Yu, Y. Preparation of nitrogen doped magnesium oxide modified biochar and its sorption efficiency of lead ions in aqueous solution. *Bioresour. Technol.* **2020**, *314*, 123708.

(45) Zhu, Y. W.; Gao, J. H.; Sun, F.; Gao, J. H.; Wu, S. H.; Qin, Y. K. Preparation of activated carbons for SO_2 adsorption by CO_2 and steam activation. *J. Taiwan Inst. Chem. Eng.* **2012**, *43*, 112−119.

(46) Pranata Putra, W.; Kamari, A.; Najiah Mohd Yusoff, S.; Fauziah Ishak, C.; Mohamed, A.; Hashim, N.; Md Isa, I. Biosorption of Cu(II), Pb(II) and Zn(II) ions from aqueous solutions using selected waste materials: adsorption and characterisation studies. *J. Encapsulation Adsorpt. Sci.* **2014**, *04*, 25−35.

(47) Zhou, Y.; Gao, B.; Zimmerman, A. R.; Fang, J.; Sun, Y.; Cao, X. Sorption of heavy metals on chitosan-modified biochars and its biological effects. *Chem. Eng. J.* **2013**, *231*, 512−518.

(48) Ding, W.; Dong, X.; Ime, I. M.; Gao, B.; Ma, L. Q. Pyrolytic temperatures impact lead sorption mechanisms by bagasse biochars. *Chemosphere* **2014**, *105*, 68−74.

(49) Pietrzak, R. XPS study and physico-chemical properties of nitrogen-enriched microporous activated carbon from high volatile bituminous coal. *Fuel* **2009**, *88*, 1871−1877.

(50) Yang, K.; Peng, J.; Xia, H.; Zhang, L.; Srinivasakannan, C.; Guo, S. Textural characteristics of activated carbon by single step CO_2 activation from coconut shells. *J. Taiwan Inst. Chem. Eng.* **2010**, *41*, 367−372.